

## Orientation of carbon nanotubes in a sheared polymer melt

E. K. Hobbie,<sup>a)</sup> H. Wang, H. Kim,<sup>b)</sup> and S. Lin-Gibson

*National Institute of Standards and Technology, Gaithersburg, Maryland 20899*

E. A. Grulke

*Advanced Carbon Materials Center, University of Kentucky, Lexington, Kentucky 40506*

(Received 6 August 2002; accepted 29 January 2003; published 2 April 2003)

Optical measurements of the shear response of semidilute dispersions of polymer-dispersed multiwalled carbon nanotubes are presented. For a weakly elastic polymer melt, the data suggest that the semiflexible tubes orient along the direction of flow at low shear stress, with a transition to vorticity alignment above a critical shear stress,  $\sigma_c$ , corresponding to a critical Deborah number of approximately 0.15. In contrast, data for a highly elastic polymer solution suggest that the tubes orient with the flow field at high shear rates, in the limit of large Deborah number. The measurements are in qualitative agreement with previous experimental and theoretical studies of fiber orientation in elastic fluids under simple shear flow. © 2003 American Institute of Physics. [DOI: 10.1063/1.1562161]

### INTRODUCTION

Nanocomposite materials engineered from polymers and carbon nanotubes offer the promise of polymer composites with greatly enhanced electrical, thermal, optical, and structural properties. As inorganic filler in a polymer matrix, the anisotropy of carbon nanotubes makes them structurally unique, in that the tube diameter can be the same order of magnitude as the radius of gyration of the polymer,<sup>1</sup> yet the aspect ratio of the tubes can be exceptionally large<sup>2</sup> while the tubes themselves can exhibit extreme mechanical strength.<sup>3</sup> In any type of extrusion or mechanical mixing process that one might envision, efficient bulk processing of nanotube-polymer composites will depend in part on a detailed understanding of the response of polymer-nanotube melts to simple steady shear flow. Of particular interest are how the shear flow orients the semiflexible nanotubes, which are essentially microscopic fibers, and how this orientation depends on the elasticity of the host polymeric fluid and hydrodynamic tube-tube interactions.

A theoretical treatment of a rigid rod under simple shear flow in a viscous fluid gives the so-called “Jeffery orbit” in which the rod undergoes a precession about the vorticity axis.<sup>4,5</sup> The orbits are characterized by an orbit constant  $C$  describing the shape of the trajectory, where  $C=0$  corresponds to perfect alignment along the vorticity axis and  $C=\infty$  corresponds to circular rotation within the flow-gradient plane. For isolated rods,  $C$  is not uniquely determined by the shear rate, but depends on the initial conditions.<sup>5</sup> The particle aspect ratio, which for nanotubes is potentially quite large, is also an important factor in the analysis of such motions, and we note that for very long slender rods, the majority of the orbit is predicted to be spent aligned with the flow field.<sup>6</sup> For

a suspension of such particles, the dilute limit is defined as  $nL^3 < 1$ , where  $n$  is the number of particles per unit volume and  $L$  is the fiber length. Observations of particle motion in dilute rod-like suspensions under shear suggest a director distribution that appears broadly peaked around the flow direction when viewed in the flow-vorticity plane.<sup>7</sup> In both dilute and semidilute suspensions (where the latter is defined by  $nL^3 > 1$  and  $nL^2d < 1$ , where  $d$  is the fiber diameter), the role of hydrodynamic interactions in determining the distribution of orbit constants, and hence the overall orientation of the fibers, has been studied and clarified both computationally and experimentally.<sup>8,9</sup> In the semi-dilute regime of interest, hydrodynamic tube-tube interactions are significant.<sup>9</sup>

Although the above observations apply to semidilute dispersions in purely viscous fluids, the scenario for fibers suspended in a viscoelastic polymer melt is somewhat different. For fibers suspended in a weakly elastic fluid, both theory and experiment appear to be consistent with shear-induced orientation along the vorticity axis,<sup>10–12</sup> while fibers in suspended in highly elastic fluids tend to align along the flow direction under strong shear.<sup>13–15</sup> An interesting question is the extent to which the shear response of nanotubes in a viscoelastic melt is identical to that of macroscopic fibers, which can be up to three orders of magnitude larger in diameter. In this paper, we present optical measurements of the shear response of semidilute suspensions of polymer-dispersed (non-Brownian) multiwalled carbon nanotubes. For a weakly elastic polymer melt, the data suggest that tubes orient along the direction of flow at low shear stress, with a transition to broad vorticity alignment above a critical shear stress,  $\sigma_c$ , corresponding to a Deborah number of approximately 0.15. In contrast, data for a highly elastic polymer solution suggest that the tubes orient along the flow direction in the limit of strong shear. In both the weakly and highly elastic limits, the measurements are in qualitative agreement with previous experimental and theoretical studies of fiber orientation in elastic fluids under simple shear.

<sup>a)</sup> Author to whom correspondence should be addressed. Electronic mail: erik.hobbie@nist.gov

<sup>b)</sup> Department of Chemistry, Kyunghee University, Yongin, Kyungkido, Korea 449-701.

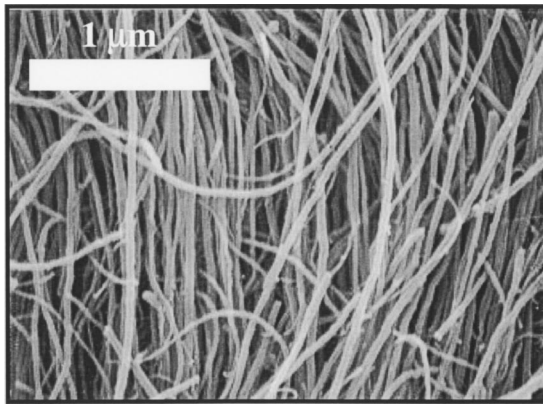


FIG. 1. Electron micrograph of typical multi-walled carbon nanotubes (MWNTs) used in the study, where the white scale bar in the upper left corner represents  $1\ \mu\text{m}$ . The tubes are semi-flexible nanofibers with an extremely large aspect ratio, a persistence length on the order of  $1\text{--}10\ \mu\text{m}$ , and an average diameter of  $50\ \text{nm}$ .

## MATERIALS AND METHODS

Details of the optical technique applied to multiwalled carbon nanotube (MWNT) suspensions under shear, as well as details of the MWNT growth procedure, will be discussed elsewhere, and here we give a brief overview. A typical electron micrograph of the nanotubes is shown in Fig. 1. Based on such measurements, the tubes have a mean diameter  $d \approx 50\ \text{nm}$  with  $M_w/M_n = 1.10$ , and based on optical microscopy measurements ( $200\times$  magnification, after polymer dispersion), the tubes have a mean length  $L \approx 12\ \mu\text{m}$  with  $M_w/M_n = 1.84$ . The data shown here are for tubes in polybutadiene (PB) of molecular weight  $M_n = 5.1 \times 10^4$ , with  $M_w/M_n = 1.04$ , but we have also measured the shear response of MWNT-dispersions in elastic Boger fluids of low-molecular-weight ( $M_n = 800$ ) polyisobutylene (PIB) containing  $0.1\%$  by mass high-molecular-weight ( $M_n = 10^6$ ) PIB. To disperse the tubes in a polymeric fluid, we dissolved  $2\ \text{g}$  of low-molecular-weight succinimide dispersant in  $600\ \text{ml}$  of toluene and mechanically mixed in  $2\ \text{g}$  of nanotubes. This solution was then sonicated for  $30\ \text{min}$ , after which aggregates and impurities were allowed to settle out. The PB and PIB are soluble in toluene, and  $1.7 \times 10^{-3}$  mass fraction MWNT dispersions were prepared by dissolving the appropriate amount of polymer (plus  $0.005$  mass fraction Good-year Wingstay #29 antioxidant in the case of PB) in the MWNT/toluene suspensions. The polymer solutions were then stirred for  $24\ \text{h}$  and the solvent removed. The final dispersions are semidilute, with  $nL^3 \approx 54$  and  $nL^2d \approx 0.23$ .

The shear light-scattering/microscopy instrument is described in detail elsewhere.<sup>16</sup> The flow direction is along the  $x$  axis, the gradient direction is along the  $y$  axis, and the vorticity direction is along the  $z$  axis. The optical measurements are taken in the  $x$ - $z$  plane. The sample is placed between two quartz plates, the upper of which rotates at a controlled angular speed. The gap between the plates was varied between  $200$  and  $400\ \mu\text{m}$ , and the rotation speed was controlled to vary the shear rate,  $\dot{\gamma} = \partial v_x / \partial y$ , at a fixed point of observation  $2\ \text{cm}$  from the center of the  $4\ \text{cm}$  (radius) plates, where the local flow is simple shear. A Rheometrics Scien-

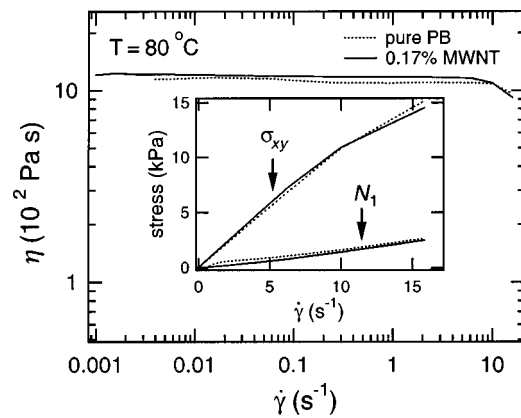


FIG. 2. The shear viscosity ( $\eta$ , main panel), shear stress ( $\sigma_{xy}$ , inset), and first normal stress difference ( $N_1$ , inset) as a function of shear rate at  $T = 80^\circ\text{C}$  for both a pure PB melt and a  $1.7 \times 10^{-3}$  mass fraction MWNT melt. Neither melt exhibits any significant regime of shear thinning, and in both melts the shear stress is a factor of five larger than the first normal stress difference.

tific Ares rheometer in a cone-and-plate geometry ( $0.1$  rad cone angle,  $\text{gap} = 0.05\ \text{mm}$ ) was used for steady-shear measurements of the viscosity ( $\eta$ ), shear stress ( $\sigma_{xy}$ ), and first normal stress difference ( $N_1$ ). A Rheometrics Scientific SR-5000 rheometer in parallel-plate geometry ( $\text{gap} = 0.4\ \text{mm}$ ) was used for dynamic measurements of  $G'(\omega)$  and  $G''(\omega)$ , the storage and loss modulus of the melt, respectively, as a function of angular frequency,  $\omega$ . All measurements were performed with  $25\ \text{mm}$  diameter fixtures, the temperature was controlled to  $\pm 0.5\ \text{K}$ , and the measurements were carried out under a nitrogen atmosphere to limit any thermal degradation of the polymers. The Reynolds number of the flow is  $Re \approx \dot{\gamma} \ell^2 \rho / \eta$  where  $\ell$  is the width of the gap, and  $\rho$  and  $\eta$  are the density and viscosity, respectively, of the polymer. At the highest  $\dot{\gamma}$  and lowest  $\eta$  encountered, we estimate that  $Re < 3 \times 10^{-3}$  and inertial effects are negligible.

Steady-shear rheology data at  $T = 80^\circ\text{C}$  for both a pure PB melt and a  $0.17\%$  MWNT by mass PB melt are shown in Fig. 2. The tubes are sufficiently dilute as to exhibit limited rheological signal. At a shear stress of  $15\ \text{kPa}$  ( $80^\circ\text{C}$ ), the first normal stress difference is a factor of five smaller than the shear stress, consistent with a PB melt that is “weakly elastic.” The low-shear viscosity of the pure PB is  $\eta \approx 4300, 1200,$  and  $540\ \text{Pa}\cdot\text{s}$  at  $T = 40, 80,$  and  $120^\circ\text{C}$ , respectively. From a linear Maxwell analysis of the viscoelastic response we obtain a relaxation time,  $\tau \approx \lim_{\omega \rightarrow 0} G' / (\omega G'') \approx \lim_{\dot{\gamma} \rightarrow 0} N_1 / (2\eta \dot{\gamma}^2)$ , where  $\tau \approx 0.018, 0.005,$  and  $0.0017\ \text{s}$  for pure PB at  $T = 40, 80,$  and  $120^\circ\text{C}$ , respectively. The Deborah number,  $De$ , then follows via the definition  $De = \tau \dot{\gamma}$ . As described above, we also prepared semidilute MWNT dispersions in an elastic Boger fluid of PIB, the shear response of which we will discuss briefly in the conclusion of this paper. At room temperature ( $25^\circ\text{C}$ ), the elastic PIB melts exhibit a steady shear viscosity of approximately  $13.5\ \text{Pa}\cdot\text{s}$  and a first normal stress difference,  $N_1$ , that varies from approximately  $1.5\ \text{Pa}$  at  $0.8\ \text{s}^{-1}$  to around  $2.15\ \text{kPa}$  at  $10\ \text{s}^{-1}$ , with an estimated linear relaxation time of  $\tau \approx 0.1\ \text{s}$ .

Because of their size and persistence length (on the order

of 1–10  $\mu\text{m}$ ), small-angle light scattering ( $\lambda=632.8\text{ nm}$ ) is ideal for probing the structure and orientation of the tubes over the range of scattered wave vector  $0.5\text{ }\mu\text{m}^{-1} < q < 5\text{ }\mu\text{m}^{-1}$ , corresponding to the range of length scales  $100\text{ nm} < 2\pi/q < 12\text{ }\mu\text{m}$ . The tubes are optically anisotropic,<sup>17</sup> and we thus employ depolarized light scattering, with the polarization of the incident beam denoted  $\mathbf{s}$  and the polarization of the analyzer  $\mathbf{p}$ . In this study we measure the four configurations  $hh(\mathbf{s}=\hat{\mathbf{x}}, \mathbf{p}=\hat{\mathbf{x}})$ ,  $vv(\mathbf{s}=\hat{\mathbf{z}}, \mathbf{p}=\hat{\mathbf{z}})$ ,  $hv(\mathbf{s}=\hat{\mathbf{x}}, \mathbf{p}=\hat{\mathbf{z}})$ , and  $vh(\mathbf{s}=\hat{\mathbf{z}}, \mathbf{p}=\hat{\mathbf{x}})$ , where  $\hat{\mathbf{x}}$  and  $\hat{\mathbf{z}}$  define the flow and vorticity directions, respectively. Explicitly, the four structure factors are

$$S_{hh}(\mathbf{q}) \propto \left| \sum_k [\delta(\hat{\mathbf{n}}_k \cdot \hat{\mathbf{x}})^2 + (\alpha - \frac{1}{3}\delta)] e^{i\mathbf{q} \cdot \mathbf{r}_k} f_k(\mathbf{q}) \right|^2, \quad (1)$$

$$S_{vv}(\mathbf{q}) \propto \left| \sum_k [\delta(\hat{\mathbf{n}}_k \cdot \hat{\mathbf{z}})^2 + (\alpha - \frac{1}{3}\delta)] e^{i\mathbf{q} \cdot \mathbf{r}_k} f_k(\mathbf{q}) \right|^2, \quad (2)$$

and

$$S_{vh}(\mathbf{q}) = S_{hv}(\mathbf{q}) \propto \left| \sum_k \delta(\hat{\mathbf{n}}_k \cdot \hat{\mathbf{x}})(\hat{\mathbf{n}}_k \cdot \hat{\mathbf{z}}) e^{i\mathbf{q} \cdot \mathbf{r}_k} f_k(\mathbf{q}) \right|^2, \quad (3)$$

where the index  $k$  runs over all of the tubes in the suspension, with  $\mathbf{r}_k$  and  $\hat{\mathbf{n}}_k$  denoting the centroid and mean director, respectively, of the  $k$ th tube. The amplitude  $f_k(\mathbf{q}) \propto \sum_j e^{i\mathbf{q} \cdot \mathbf{r}_{kj}}$ , where  $\mathbf{r}_{kj}$  locates the  $j$ th element of the  $k$ th tube with respect to  $\mathbf{r}_k$ , contains information about the effective shape of the tubes. We assume that  $\alpha$  and  $\delta$  are homogeneous throughout the sample.<sup>17</sup> From the above expressions, we see that the  $hh$  scattering intensity is sensitive to orientation of the tubes along the flow direction, the  $vv$  intensity is sensitive to orientation of the tubes along the vorticity direction, and the  $hv$  ( $vh$ ) intensity is sensitive to orientation of the tubes at  $45^\circ$  in the flow-vorticity plane. When confined to the 200–400  $\mu\text{m}$  gap of the optical shear cell, the melts appear transparent dark gray. Digital video microscopy is simultaneously employed<sup>16</sup> to obtain real-space micrographs (width = 200  $\mu\text{m}$ ) in which the tubes appear as faint anisotropic dark regions that provide an additional measure of orientation.

## RESULTS AND DISCUSSION

Figure 3 shows optical data for a dilute PB/MWNT melt ( $1.7 \times 10^{-3}$  mass fraction MWNT) at  $T=40^\circ\text{C}$  and  $\dot{\gamma}=0.02\text{ s}^{-1}$ , where the width of the micrograph is 100  $\mu\text{m}$ . The anisotropy is weak, and the shape of the  $hh$  and  $vv$  scattering patterns are nearly related by a  $90^\circ$  rotation about the gradient ( $y$ ) direction. The  $hv$  and  $vh$  patterns are nearly symmetric 4-lobed shapes, with the  $45^\circ$  axis being characteristic of an isotropic director distribution. Tubes in the focal plane appear as faint, dark, anisotropic shapes in the optical micrographs. Figure 4 shows optical data for the melt depicted in Fig. 3 at  $\dot{\gamma}=1.0\text{ s}^{-1}$ . Orientation of the tubes along the flow direction is evident in the anisotropy of the  $hh$  and  $vv$  patterns [relative to Fig. 3], the deviation from  $45^\circ$  in the  $hv$  and  $vh$  patterns, and the orientation of shadow patterns in the optical micrographs. With most of the tubes aligned along  $\hat{\mathbf{x}}$ , the  $vv$  pattern in Fig. 4 reflects scattering from the

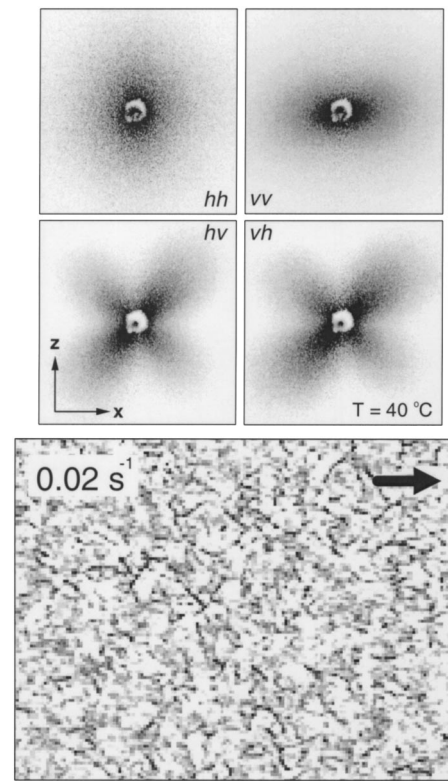


FIG. 3. Light-scattering/micrograph pair for a weakly sheared ( $\dot{\gamma}=0.02\text{ s}^{-1}$ ) PB/MWNT melt prepared at  $1.7 \times 10^{-3}$  mass fraction MWNT at a temperature of  $40^\circ\text{C}$ , where the measurements are taken in the flow-vorticity ( $x$ - $z$ ) plane, with the flow direction as indicated. The scattering intensity depends on the relative configuration of the incident and analyzing polarizer, and in this study we measure the four configurations  $hh$ ,  $vv$ ,  $hv$ , and  $vh$ , as described in the text. The width of the micrograph is 100  $\mu\text{m}$  and the light-scattering pattern subtends an angle of  $\pm 27^\circ$ . Tubes lying in the optical focal plane are apparent as extended faint black shadow patterns in the micrographs.

component of tube orientation along  $\hat{\mathbf{z}}$ , suggesting structure that is somewhat broadly peaked around  $\hat{\mathbf{x}}$ . Figure 5 shows data for same melt at  $\dot{\gamma}=50\text{ s}^{-1}$ . Broad orientation of the tubes along the vorticity axis is now evident in the anisotropy of the  $hh$  and  $vv$  patterns (inverted relative to that in Fig. 4), and in the deviation from  $45^\circ$  in the  $hv$  and  $vh$  patterns. Orientation of the tubes along  $\hat{\mathbf{z}}$  is also evident in the left panel of the micrograph, which was taken in the middle of the gap, while near the wall (right panel) the tubes exhibit a degree of alignment along the flow direction. This bimodality is evident in the  $hh$  light scattering pattern in as a faint vertical streak. Anisotropy between the first and second quadrant in the intensity of lobes in the  $vh$  and  $hv$  patterns is an experimental artifact that emerges at high  $\dot{\gamma}$ .

To infer information about the orientation of the nanotubes from the  $hh$  and  $vv$  light-scattering patterns, we consider projections of these structure factors along the flow ( $x$ ) and vorticity ( $z$ ) directions. There are then four characteristic length scales contained in the  $hh$  and  $vv$  scattering patterns;  $\xi_{hx}$ ,  $\xi_{hz}$ ,  $\xi_{vx}$ , and  $\xi_{vz}$ . To extract these, we fit the data to  $S(q_i) \approx S(0) \exp(-\xi_i^2 q_i^2/2)$  in the low- $q$  limit,<sup>18</sup> and Fig. 6 shows the four length scales as a function of  $\dot{\gamma}$  for the  $1.7 \times 10^{-3}$  mass fraction MWNT PB melt at (a)  $40^\circ\text{C}$ , (b)  $80^\circ\text{C}$ , and (c)  $120^\circ\text{C}$ . For the  $hh$  pattern, orientation of the

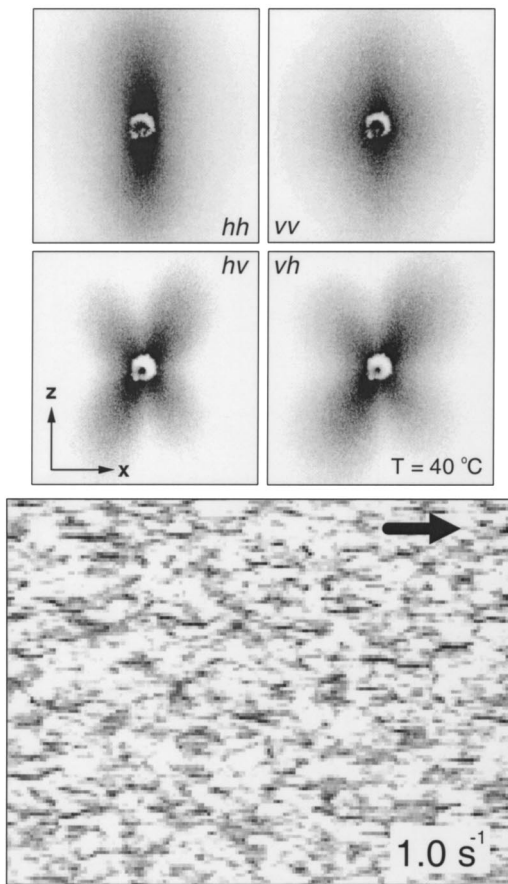


FIG. 4. Light-scattering/micrograph pair for a PB/MWNT dispersion ( $1.7 \times 10^{-3}$  mass fraction MWNT,  $T=40^\circ\text{C}$ ) at a shear rate of  $1.0 \text{ s}^{-1}$ . Orientation of the tubes along the flow direction is evident in the anisotropy of the  $hh$  and  $vv$  patterns, and in the orientation of the intensity lobes in the  $hv$  and  $vh$  patterns. The mean orientation of the tubes is also evident in the micrograph. The geometry is the same as that in Fig. 3 and the width of the micrograph is  $100 \mu\text{m}$ .

tubes along the flow direction leads to a decrease in  $\xi_{hz}$ , while  $\xi_{hx}$  remains saturated at around  $0.7 \mu\text{m}$ . For the  $vv$  pattern, orientation of the tubes along the direction of flow is apparent as a shear-induced increase in  $\xi_{vx}$  and a shear-induced decrease in  $\xi_{vz}$ . The transition from flow to vorticity alignment is apparent as a shear-induced decrease in  $\xi_{hx}$  and  $\xi_{vx}$ , and a shear-induced increase in  $\xi_{hz}$  and  $\xi_{vz}$ , which occurs at higher shear rates as the temperature increases. Plotting the correlation lengths  $\xi_{hx}$  and  $\xi_{hz}$  as a function of Deborah number for all of the temperatures superimposes the transitions, as shown in Fig. 7, and reveals the transition to vorticity alignment in the vicinity of  $De \approx 0.15$ . Analogous plots as a function of shear stress look quite similar and suggest the transition occurs at a critical shear stress of  $10\text{--}15 \text{ kPa}$ , which we denote  $\sigma_c$ .

Information about the orientation of the tubes is also contained in the angles locating the lobes of maximum intensity in  $S_{hv}(\mathbf{q})$  and  $S_{vh}(\mathbf{q})$ , which we denote  $\phi$ . From a relatively crude but effective model consisting of two-dimensional (2D) rectangular shapes in the  $x$ - $z$  plane,<sup>16</sup> one can easily derive the simple but general relation  $\phi = \pm(\pi/2 - \theta_m) \pm n\pi$  ( $n=0,1,2,\dots$ ), where the angle  $\theta_m$  locates the maximum in the effective probability distribution function

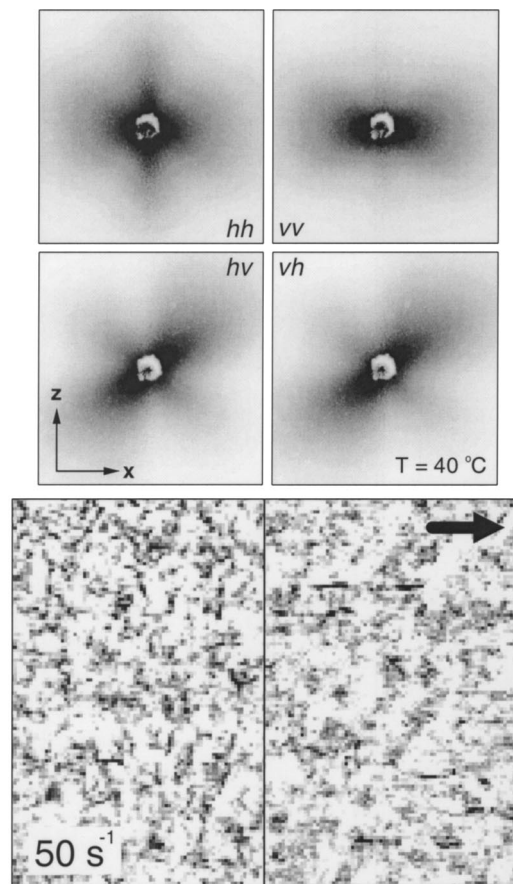


FIG. 5. Light-scattering/micrograph pair for a PB dispersion ( $1.7 \times 10^{-3}$  mass fraction MWNT,  $T=40^\circ\text{C}$ ) at a shear rate of  $50 \text{ s}^{-1}$ . Broad orientation of the tubes along the vorticity direction is evident in the anisotropy of the  $hh$  and  $vv$  patterns, and in the orientation of the intensity lobes in the  $hv$  and  $vh$  patterns (see Fig. 4 for comparison). Orientation of the tubes along the vorticity axis is also evident in the left panel of the micrograph, which was taken in the middle of the gap, while near the wall (right panel) the tubes exhibit alignment along the flow direction. This bimodality is evident in the  $hh$  light scattering pattern as a faint vertical streak. The geometry is the same as that in Figs. 3 and 4, and the width of each panel is  $50 \mu\text{m}$ .

$p(\theta)\sin^2\theta\cos^2\theta$ . Here,  $p(\theta)$  is a tilt-angle distribution function, with  $\theta$  defined as the angle between the projection of the tube director into the  $x$ - $z$  plane and the flow ( $x$ ) direction. For an isotropic system [ $p(\theta) = \text{const}$ ], the maxima thus occur at odd multiples of  $45^\circ$ , as noted above. Figure 8(a) shows the angle  $\theta_m(\dot{\gamma})$  inferred from the  $hv$  and  $vh$  light-scattering data for the  $0.17\%$  MWNT by mass PB melt at each of the three temperatures, where the inset shows the  $vh$  pattern at  $\dot{\gamma}=0.02 \text{ s}^{-1}$  and  $T=40^\circ\text{C}$ , with the angles  $\theta_m$  and  $\phi$  as indicated. As the tubes orient with the flow direction, the orientation of the scattering lobes thus evolves toward the vorticity direction, and as the tubes align with the vorticity axis, the scattering lobes move toward the flow direction, reflecting the inverted nature of the response in  $q$ -space. The effect of varying temperature is clearly evident at the four highest shear rates in Fig. 8(a), where the shear rate at which  $\theta_m$  becomes larger than  $\pi/4$  increases with increasing temperature. Multiplying  $\dot{\gamma}$  by the viscosity converts the horizontal axis in Fig. 8(a) to shear stress [Fig. 8(b)] and collapses the positive slope data for all three temperatures into a

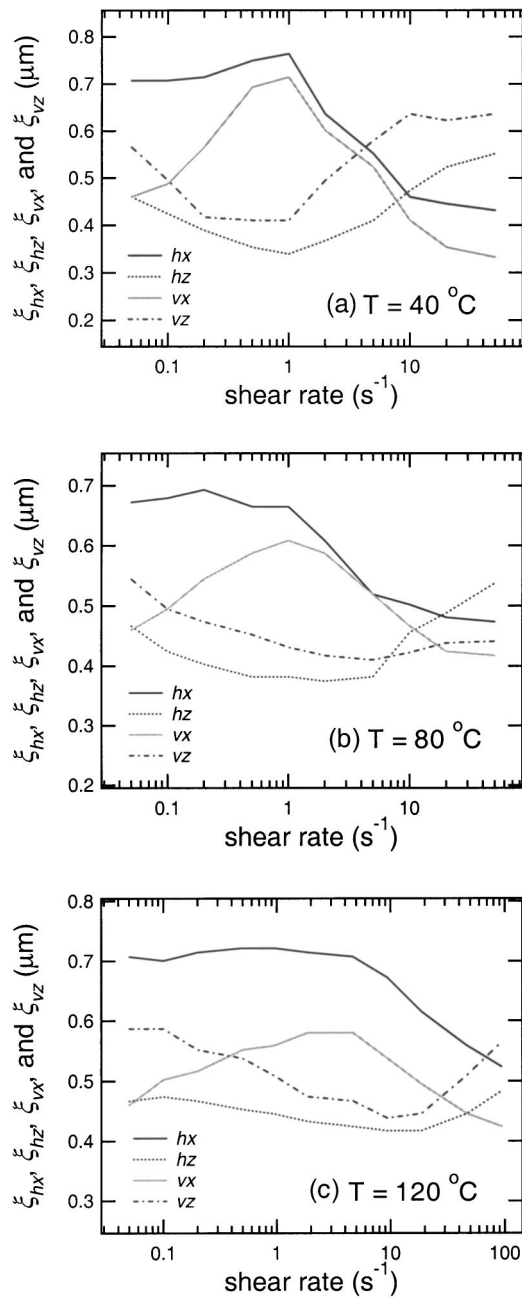


FIG. 6. The four characteristic length scales determined from the  $hh$  and  $vv$  light-scattering patterns ( $\xi_{hx}$ ,  $\xi_{hz}$ ,  $\xi_{vx}$ , and  $\xi_{vz}$ ) as a function of shear rate for a PB/MWNT melt prepared at  $1.7 \times 10^{-3}$  mass fraction MWNT at temperatures of (a) 40 °C, (b) 80 °C, and (c) 120 °C. The transition from flow alignment to vorticity alignment is apparent as a shear-induced decrease in  $\xi_{hx}$  and  $\xi_{vx}$ , and a shear-induced increase in  $\xi_{hz}$  and  $\xi_{vz}$ .

single trend. These measurements also suggest that the transition to vorticity alignment occurs at a critical shear stress ( $\sigma_c$ ) of approximately 10–15 kPa. Converting the horizontal axis in Fig. 8(a) to  $De$  has the same effect, as shown in Fig. 8(c).

Turning now to the real-space data provided by the optical micrographs, Fig. 9(a) shows the tilt-angle distribution functions,  $p(\theta)$ , obtained for conditions above and below the transition from flow to vorticity alignment. The histograms have been made symmetric with respect to  $\theta=90^\circ$  to eliminate slight residual anisotropy in the ensembles, which con-

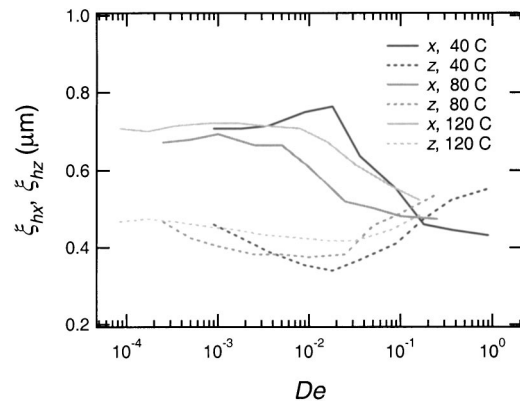


FIG. 7. A universal plot of the two correlation lengths  $\xi_{hx}$  and  $\xi_{hz}$  as a function of Deborah number for the three temperatures considered, where the transition to vorticity alignment emerges in the vicinity of  $De \approx 0.15$ . Universal plots as a function of shear stress look similar, and suggest the transition occurs at 10–15 kPa.

tain on the order of 4000 individual tube shapes. The angles are obtained by finding the axis of least-moment-of-inertia for each of the shapes representing distinct nanotubes in the micrographs.<sup>16</sup> Based on these distributions, the effective probability distributions relevant to the  $hv$  and  $vh$  scattering,  $p(\theta)\sin^2\theta\cos^2\theta$ , are easily computed and are shown in Fig. 9(b). The dark triangles indicate the locations of the maxima,  $\theta_m$ , suggested by the analysis of the  $hv$  and  $vh$  light-scattering patterns discussed above. The transition to vorticity alignment at high shear stress is clearly evident in Fig. 9(a) as a shift in the position of the most probable tilt angle, and in Fig. 9(b) as a shift in the peak position with respect to  $\pi/4$ . As mentioned above, the data suggest that the director distribution at high shear stress is actually weakly bimodal, as evidenced by a vertical stripe in the  $hh$  scattering pattern in Fig. 5 and weak secondary maxima in  $p(\theta)$  at  $\theta=0$  and  $\pi$  [Fig. 9(a)]. Based on optical images obtained at different focal depths in the vicinity of the bottom (stationary) plate, we attribute this to wall effects; tubes very close to the bottom wall exhibited a tendency to be aligned with the flow direction, even when tubes in the bulk tend to exhibit vorticity elongation.

## CONCLUSIONS

Optical measurements of the shear response of semidilute ensembles of multi-walled carbon nanotubes dispersed in a weakly elastic polymer are presented and discussed. Below a critical shear stress ( $\sigma_c$ ) the measurements suggest that the tubes become broadly oriented along the direction of flow, while above  $\sigma_c$ , the data suggest a transition in which the tubes become broadly oriented along the vorticity axis. When cast in terms of a Deborah number, these observations appear to be consistent with previous experimental and theoretical work on the orientation of fibers in weakly elastic fluids,<sup>10–12</sup> which also suggest vorticity alignment. It is interesting to ask how this trend might extrapolate to higher Deborah number. As mentioned above, we also prepared semidilute (0.17% MWNT by mass) dispersions in an elastic (PIB) Boger fluid. Such measurements, which were per-

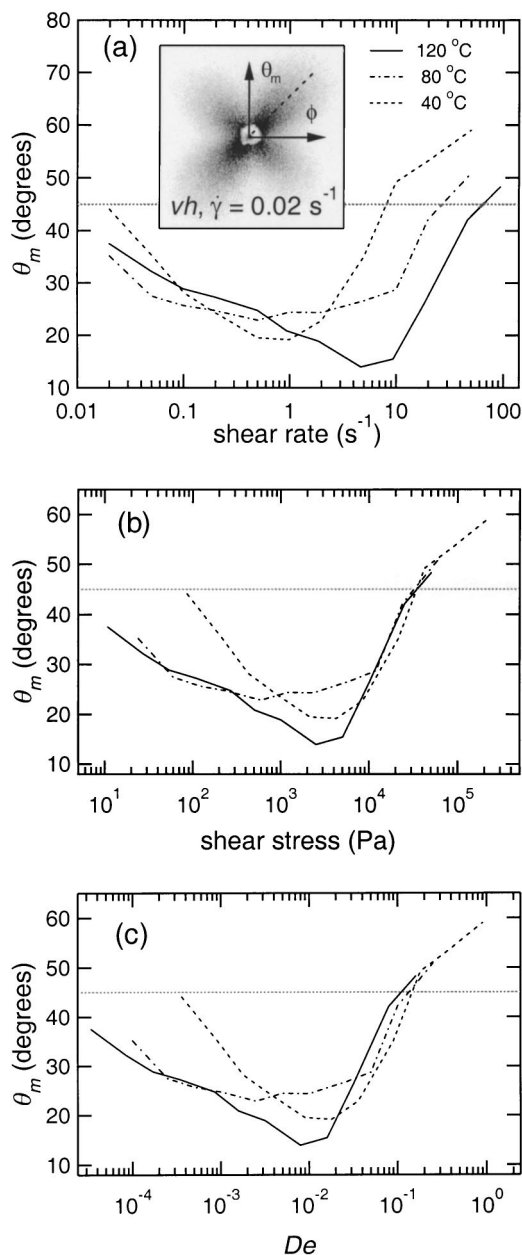


FIG. 8. (a) The angle  $\theta_m$  as a function of shear rate for the  $1.7 \times 10^{-3}$  mass fraction MWNT sample under consideration, where  $\theta_m = 45^\circ$  corresponds to an isotropic configuration. The inset shows the  $vh$  light-scattering pattern at  $\dot{\gamma} = 0.02 \text{ s}^{-1}$ , with the angles  $\theta_m$  and  $\phi$  as indicated. With increasing temperature, the transition from flow alignment to vorticity alignment occurs at higher shear rate, reflecting the decreased viscosity of the PB matrix. (b) The same data plotted as a function of shear stress, and (c) the same data plotted as a function of Deborah number.

formed at  $25^\circ\text{C}$ , are complicated by the fact that the viscosity of the PIB fluid is low enough for weak shear to induce aggregation of the non-Brownian nanofibers, the microscale analog of a phenomenon frequently encountered in the processing of fiber suspensions.<sup>19</sup> Although details of this flow-induced aggregation will be discussed in detail elsewhere, we note here that above a shear stress of around 300 Pa, the MWNT aggregates start to “melt,” and optical measurements of the orientation of individual tubes in semidilute suspensions under such conditions are similar to those de-

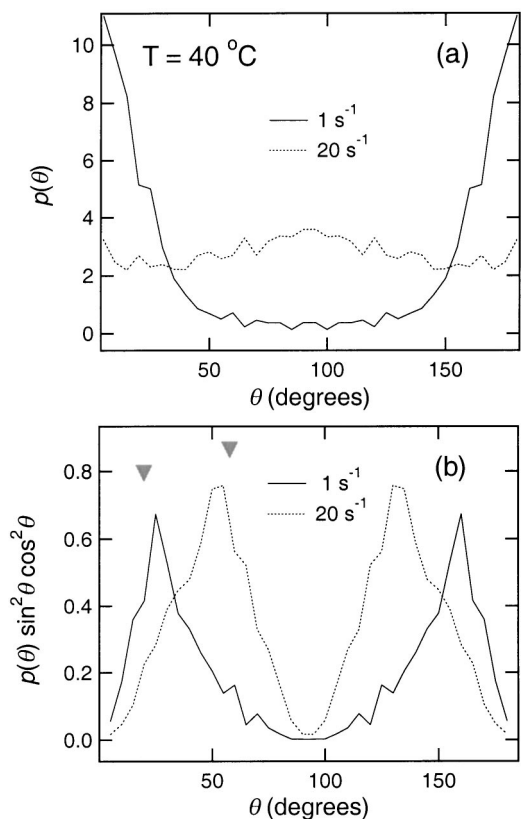


FIG. 9. (a) Tilt-angle distribution functions,  $p(\theta)$ , determined from the optical micrographs for the melt depicted in Figs. 3–5 ( $1.7 \times 10^{-3}$  mass fraction MWNT,  $T = 40^\circ\text{C}$ ). The histograms have been made symmetric with respect to  $\theta = 90^\circ$  to eliminate very weak residual anisotropy in the ensembles. (b) Effective probability distributions (relevant for the  $hv$  and  $vh$  light-scattering patterns) based on the real-space distributions shown in (a). The dark triangles indicate the location of the maxima suggested by the  $hv$  and  $vh$  light-scattering patterns.

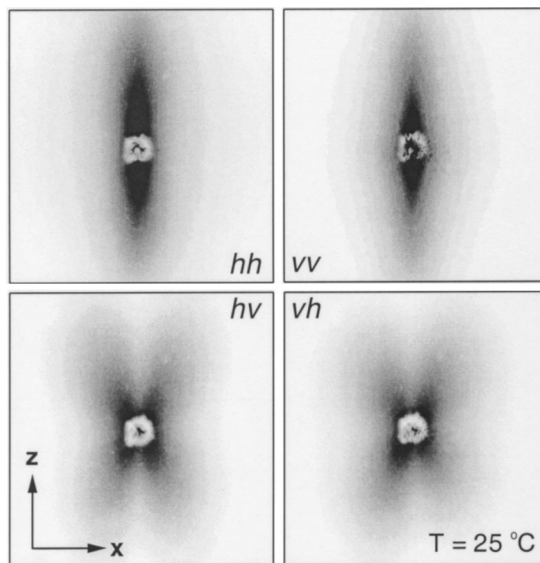


FIG. 10. Light-scattering patterns for a PIB/MWNT dispersion ( $1.7 \times 10^{-3}$  mass fraction MWNT,  $T = 25^\circ\text{C}$ ) at a shear rate of  $100 \text{ s}^{-1}$  ( $De \approx 10$ ). Orientation of the tubes along the flow direction is evident in the anisotropy of the  $hh$  and  $vv$  patterns, and in the orientation of the intensity lobes in the  $hv$  and  $vh$  patterns. The geometry is the same as that depicted in Fig. 4.

picted in Fig. 4, suggesting flow alignment for  $1 < De < 20$ . We show an example of this behavior in Fig. 10, which depicts the four light scattering patterns obtained at  $100 \text{ s}^{-1}$  for a 0.17% MWNT by mass dispersion in the elastic Boger fluid, corresponding to a Deborah number of around 10. These observations are consistent with previous work on fibers suspended in highly elastic fluids,<sup>13–15</sup> which suggest fiber orientation along the direction of flow at high  $De$ . For the weakly elastic PB melts, we note that the shear response up to the critical stress, or Deborah number, is analogous to the shear response of semi-dilute fiber suspensions in purely viscous fluids, with tube orientation along the direction of flow.<sup>7–9</sup> Intuitively, one would expect the shear response of non-Brownian fibers to be independent of their size, and our measurements on this system appear to be in good agreement with this perception.

### ACKNOWLEDGMENTS

We would like to thank J. A. Pathak for assistance with the Boger fluid preparation and rheology. One of us (H.K.) would like to acknowledge financial support from Kyunghee University.

<sup>1</sup>T. W. Ebbesen, *Carbon Nanotubes* (CRC, Boca Raton, 1997).

<sup>2</sup>Z. W. Pan, S. S. Xie, B. H. Chang, C. Y. Wang, L. Lin, W. Y. Zhou, W. Z. Li, and L. X. Quian, "Very long carbon nanotubes," *Nature* (London) **394**, 631 (1998).

<sup>3</sup>B. I. Yakobson, C. J. Brabec, and J. Bernholc, "Nanomechanics of carbon tubes: Instabilities beyond linear response," *Phys. Rev. Lett.* **76**, 2511 (1996).

<sup>4</sup>G. B. Jeffery, "The motion of ellipsoidal particles immersed in a viscous fluid," *Proc. R. Soc. London, Ser. A* **102**, 161 (1922).

<sup>5</sup>B. J. Trevelyan and S. G. Mason, "Particle motions in sheared suspensions: Rotations," *J. Colloid Sci.* **6**, 354 (1951); O. L. Forgacs and S. G. Mason, "Particle motions in sheared suspensions: Spin and deformation of threadlike particles," *ibid.* **14**, 457 (1959).

<sup>6</sup>E. J. Hinch and L. G. Leal, "The effect of Brownian motion on the rheological properties of a suspension of non-spherical particles," *J. Fluid Mech.* **52**, 683 (1972).

<sup>7</sup>E. Anczurowski and S. G. Mason, "The Kinetics of flowing dispersions: Equilibrium orientations of rods and disks," *J. Colloid Interface Sci.* **23**, 533 (1967).

<sup>8</sup>C. A. Stover, D. L. Koch, and C. Cohen, "Observations of fiber orientation in simple shear flow of semi-dilute suspensions," *J. Fluid Mech.* **238**, 277 (1992).

<sup>9</sup>M. Rahnama, D. L. Koch, and E. S. G. Shaqfeh, "The effect of hydrodynamic interactions on the orientation distribution in a fiber suspension subject to simple shear flow," *Phys. Fluids* **7**, 487 (1995).

<sup>10</sup>L. G. Leal, "The slow motion of slender rod-like particles in a second-order fluid," *J. Fluid Mech.* **69**, 305 (1975).

<sup>11</sup>O. G. Harlen and D. L. Koch, "Simple shear flow of a suspension of fibers in a dilute polymer solution at high Deborah number," *J. Fluid Mech.* **252**, 187 (1993).

<sup>12</sup>Y. Iso, D. L. Koch, and C. Cohen, "Orientation in simple shear flow of semi-dilute fiber suspensions: Weakly elastic fluids," *J. Non-Newtonian Fluid Mech.* **62**, 115 (1996).

<sup>13</sup>Y. Iso, C. Cohen, and D. L. Koch, "Orientation in simple shear flow of semi-dilute fiber suspensions: Highly elastic fluids," *J. Non-Newtonian Fluid Mech.* **62**, 135 (1996).

<sup>14</sup>E. Bartram, H. L. Goldsmith, and S. G. Mason, "Particle motions in non-Newtonian media: Further observations in elasticoviscous fluids," *Rheol. Acta* **14**, 776 (1975).

<sup>15</sup>S. J. Johnson, A. Salem, and G. G. Fuller, "Dynamics of colloidal particles in sheared non-Newtonian fluids," *J. Non-Newtonian Fluid Mech.* **34**, 89 (1990).

<sup>16</sup>S. Kim, J. Yu, and C. Han, "Shear light scattering photometer with optical microscope for the study of polymer blends," *Rev. Sci. Instrum.* **67**, 3940 (1996). A more detailed discussion of the capabilities and limitations of this optical technique applied to aqueous nanotube suspensions under simple shear flow is given in E. K. Hobbie, H. Wang, H. Kim, C. C. Han, E. A. Grulke, and J. Obrzut, "Optical measurements of structure and orientation in sheared carbon-nanotube suspensions," *Rev. Sci. Instrum.* **74**, 1244 (2003).

<sup>17</sup>Any free charge in the fullerene sheets will be mobile, and the polarizability parallel to the long axis of the tube is thus expected to be larger than that normal to this axis. The overall tube director is defined by the mean orientation of the tube. In the expressions for the four structure factors given in the text, the mean polarizability and anisotropy are defined as  $\alpha = (\alpha_{\parallel} + 2\alpha_{\perp})/3$  and  $\delta = (\alpha_{\parallel} - \alpha_{\perp})$ , respectively, where  $\alpha_{\parallel}$  and  $\alpha_{\perp}$  denote the polarizability along directions parallel ( $\parallel$ ) and perpendicular ( $\perp$ ) to the director.

<sup>18</sup>The expression  $S(q_i) \approx S(0) \exp(-\xi_i^2 q_i^2/2) \approx 1 - \xi_i^2 q_i^2/2 + \dots$  is motivated by a small- $q$  expansion of the structure factors for any general model, which yields a Gaussian profile at low- $q$ . The fits include a "virtual" background that is consistently larger than the measured scattering intensity in the high- $q$  limit, suggesting that the effective background is  $q$ -dependent. The range of wave vector used in these fits is  $q < 2 \mu\text{m}^{-1}$ .

<sup>19</sup>See, for example, C. F. Schmid, L. H. Switzer, and D. J. Klingenberg, "Simulations of fiber flocculation: Effects of fiber properties and interfiber friction," *J. Rheol.* **44**, 781 (2000), and references therein.